Distance Keeping for Underwater Vehicles – Tuning Kalman Filters Using Self-Oscillations

Nikola Miskovic, Zoran Vukic, Ivan Petrovic and Matko Barisic
University of Zagreb, Faculty of Electrical Engineering and Computing
Unska 3, Zagreb, Croatia
e-mail: {nikola.miskovic, zoran.vukic, ivan.petrovic, matko.barisic}@fer.hr

***Abstract*— This paper describes the use of Kalman filtering in distance keeping for underwater vehicles. The vision-based distance keeping module has been mounted on a micro-ROV equipped with a camera. Distance from a plane-like obstacle is determined on the basis of the laser dot projections within the frame. Since these measurements are not reliable a Kalman filter is designed - unknown dynamic model parameters are determined using the self-oscillation experiments which prove to be simple and time preserving. Finally, an I-PD controller is designed based on the Kalman filter estimates. The main task of the controller is to keep the vehicle perpendicular to the surface at a desired distance.**

I. Introduction

Distance keeping for underwater vehicles has important application in practice, especially during inspection missions. These modules can be of great help for the operator while performing an inspection mission (dams, ship hulls, etc.) and are essential in fully autonomous applications. In addition to that, distance keeping can be used as an obstacle avoidance module. The main task of distance keeping algorithms is to ensure that the vehicle keeps either a predefined distance from a fixed object (during inspections) or follows a moving object keeping a safe distance. Distance keeping sensors which can be found in underwater technologies are usually sonars, distance lasers and normal lasers. The greatest advantage of sonars is that they provide accurate and detailed information on the shape as well as the position of an obstacle. However, their cost might be a problem especially if low-cost solutions are needed. Distance lasers are somewhat more appropriate cost-wise but the measurements provided are not as reliable. Normal lasers ar the cheapest option (even though at least two are necessary) but they reliability is the poorest. Also, they are commonly used with vision-based algorithms in order to determine the distance from an object. The latter type of sensor will be used in this paper. Some prior implementations of similar technology can be found in [1], [2], [3]. Due to low reliability of laser sensors, Kalman filter (KF) is an essential addition.

Kalman filtering is often used in underwater vehicles' applications. The reasons for this are numerous, [4]:

- sensors that are used often have course quantization levels and/or are noisy,
- available sensors' data have to be fused in order to obtain more confident signal values,
- control algorithms demand higher update frequency than the sensors' sampling frequency,
- estimation of unmeasurable states is needed for control purposes (velocities), etc.

Fig. 1. VideoRay ROV with vision-based distance keeping sensor

In underwater applications Kalman filter equations must include vehicle dynamics since, which cannot be neglected. This paper will demonstrate tuning Kalman filter parameters (dynamic model parameters) based on self-oscillation experiments. In [5], [6] these experiments have been used for tuning low-level controllers for underwater vehicles without using Kalman filter estimates. The method has also been applied on autonomous catamaran *Charlie* (heading and line following controllers) what is reported in [7]. The proposed methodology has been tested on a VideoRay ROV equipped with a vision-based laser distance sensor as shown in Fig. 1. The paper is organized as follows. The introductory section continues with the description of the mathematical model of distance keeping for underwater vehicles. Section 2 derives the Kalman filter while Section 3 describes the self-oscillation method used to determine surge and yaw dynamic model of the vehicle. The proposed nonlinear controller is described in Section 4 while experimental results are presented in Section 5. The paper is concluded with Section 6.

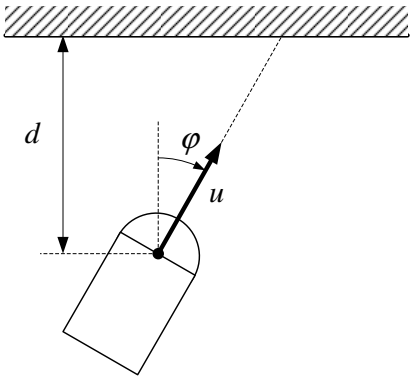

Fig. 2. Distance keeping scheme

A. Mathematical Model

The mathematical model of distance keeping is derived based on Fig. 2 and is given by the following equations:

$$\dot{u} = -\frac{k_{u|u|}}{m_{u|u|}}u|u| + \frac{1}{m_{u|u|}}\tau_X \quad (1)$$

$$\dot{r} = -\frac{k_{r|r|}}{I_{r|r|}}r|r| + \frac{1}{I_{r|r|}}\tau_N \quad (2)$$

$$\dot{\varphi} = r + v_\varphi \quad (3)$$

$$\dot{\psi} = r + v_\varphi \quad (4)$$

$$\dot{d} = -u\cos\varphi + v_d \quad (5)$$

$$\dot{v}_\varphi = 0 \quad (6)$$

$$\dot{v}_d = 0 \quad (7)$$

where u is surge speed, r yaw rate, ψ heading, τ_X surge thrust, τ_N yaw moment, φ angle and d distance relative to the plan-like surface. I_r and $k_{r|r|}$ are total yaw inertia and drag respectively, while m_u and $k_{u|u|}$ are total surge mass and drag respectively. Equations (1) and (2) represent the dynamic behavior of the vehicle while (3), (4) and (5) are kinematic equations augmented with states v_φ and v_d which represent constant disturbance that may act upon the vehicle. They can also be interpreted as terms which include all the unknown dynamics of the system. A detailed derivation of dynamic models of underwater vehicles can be found in [8] and [9].

B. Vision-Based Laser Distance Module

The vision-based laser distance module has been developed for underwater vehicles for the purpose of calculating current distance from a plane-like surface. It is placed below the vehicle and is projecting two laser dots on the surface. The integrated camera detects the dots in the field of vision and based on the relative distance of the two dots, Δx, distance from the surface, d, is calculated. Since $d = f(\Delta x)$ is a nonlinear function, calibration has to be performed.

An algorithm for finding the two dots has been developed which computational complexity does not depend on the acquired image dimensions. It is based on searching only a limited area of the image around the dots which have been found in the previous step. This significantly reduces the time required for image analysis comparing to other algorithms that search the whole image obtained from the integrated camera at every step. The algorithm is briefly described in the following:

a) Search the whole image (n x m pixels) and find two laser dots.
b) Calculate $d = f(\Delta x)$.
c) Set two square search areas (n^* x m^* pixels, $n^* < n$, $m^* < m$) around each laser dot.
d) Search the two rectangles (n^* x m^* pixels) and find two laser dots.
e) Calculate $d = f(\Delta x)$.
f) If laser dots are found, go to c).
g) If laser dots are not found, go to a).

The square search areas are sized so that under normal conditions (normal vehicle speeds) the dots will not disappear between two searching steps. If the dots disappear, the vehicle is either moving too fast (the square search areas should be larger) or something occludes laser dots and they are not visible any more.

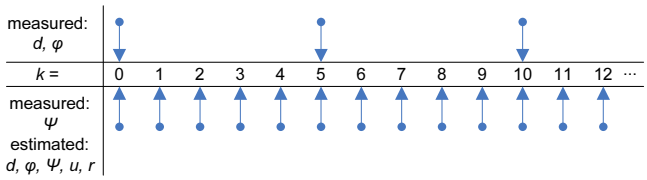

Fig. 3. Timeline of measurements and estimations

II. Kalman Filter Equations

The signals that can be measured in the mentioned case are compass heading, ψ, distance from obstacle, d, and angle with regard to the obstacle, φ, (two latter are obtained from the vision-based distance sensor). The motivation for the use of Kalman filter is dual. Firstly, estimation of unmeasurable yaw rate, r and surge speed u, which are needed for controller design. Secondly, estimation of the distance d from the surface when measurements are not available: vision-based laser module works with frequency of 2 Hz while control is performed at 10 Hz and therefore estimation is needed between two available measurements, see Fig. 3. Also, the vehicle might get too close or too far from the plane-like surface which leads to laser dots disappearing from the image - estimation in these cases is crucial for system operation.

Given the fact that the mathematical model of the vehicle given with (1) – (7) is nonlinear, extended Kalman filter (EKF) in its discrete form is used, see [4] and [10]. If the state vector is $y_k = \begin{bmatrix} u_k & r_k & \varphi_k & \psi_k & d_k & v_{\varphi,k} & v_{d,k} \end{bmatrix}^T$, discrete-time EKF prediction and correction equations are derived from the mathematical model and are presented in Table I. The minus in the superscript denotes the prediction. $\mathbf{A}$ is the Jacobian matrix in the form given with (8). Covariance matrices are preset as $\mathbf{Q} = 0.1\mathbf{I}_{7\text{x}7}$, $\mathbf{R} = diag\{0.5, 10, 0.1\}$ and $\mathbf{P}_0 = 1000\mathbf{I}_{7\text{x}7}$.

TABLE I

KALMAN FILTER EQUATIONS

Prediction equations
$u_k^- = u_{k-1} + T\beta_1 u_{k-1}\lvert u_{k-1}\rvert + T\beta_2 \tau_{X,k}$
$r_k^- = r_{k-1} + T\alpha_1 r_{k-1}\lvert r_{k-1}\rvert + T\alpha_2 \tau_{N,k}$
$\varphi_k^- = \varphi_{k-1} + T r_{k-1} + T v_{\varphi,k}$
$\psi_k^- = \psi_{k-1} + T r_{k-1} + T v_{\varphi,k}$
$d_k^- = d_{k-1} - T u_{k-1}\cos\varphi_{k-1} + T v_{d,k-1}$
$v_{\varphi,k}^- = v_{\varphi,k-1}$
$v_{d,k}^- = v_{d,k}$
$P_k^- = A_k P_{k-1} A_k^T + Q$
Correction equations
$K_k = P_k^- H_k^T \left[H_k P_k^- H_k^T + R_k\right]^{-1}$
$\hat{x}_k = \hat{x}_k^- + K_k\left[y_k - H_k \hat{x}_k^-\right]$
$P_k = \left[I - K_k H_k\right] P_k^-$

$$A_k = \mathbf{I}_{7\times 7} + T\begin{bmatrix} 2\beta_1|u_k| & 0 & 0 & 0 & 0 & 0 & 0 \\ 0 & 2\alpha_1|r_k| & 0 & 0 & 0 & 0 & 0 \\ 0 & 1 & 0 & 0 & 0 & 1 & 0 \\ 0 & 1 & 0 & 0 & 0 & 1 & 0 \\ -\cos\varphi_k & 0 & 0 & u_k\sin\varphi_k & 0 & 0 & 1 \\ 0 & 0 & 0 & 0 & 0 & 0 & 0 \\ 0 & 0 & 0 & 0 & 0 & 0 & 0 \end{bmatrix} \quad (8)$$

Measurement matrix, H_k, which appears in correction equations has a form $H_{1,k}$ when measurements from the vision-based laser module are available, and $H_{2,k}$ when measurements are not available (at times between two measurements, or when laser dots are not found), see (9) and (10).

$$H_{1,k} = \begin{bmatrix} 0 & 0 & 1 & 0 & 0 & 0 & 0 \\ 0 & 0 & 0 & 1 & 0 & 0 & 0 \\ 0 & 0 & 0 & 0 & 1 & 0 & 0 \end{bmatrix} \quad (9)$$

$$H_{2,k} = \begin{bmatrix} 0 & 0 & 0 & 0 & 0 & 0 & 0 \\ 0 & 0 & 0 & 0 & 0 & 0 & 0 \\ 0 & 0 & 0 & 1 & 0 & 0 & 0 \end{bmatrix} \quad (10)$$

The unknown dynamic model parameters which appear in Kalman equations will be identified using the procedure described in the following section.

III. IDENTIFICATION BY USE OF SELF-OSCILLATIONS (I–SO)

The idea of using self-oscillations to determine system parameters was introduced in [11]. Since then, the method has been applied in process industry for tuning controllers. First application of the method in marine control was reported in [5], [6] and [12], where it was applied for identification of an underwater vehicle dynamic model. Since then, it has been applied for heading controller tuning of marine surface vehicles, see [7] for details.

The I-SO experiment was done in closed loop which consists of a nonlinear element, the process and a unity feedback as shown in Fig. 5. The method is based upon forcing the system into self-oscillations – the magnitude X_m and frequency ω of the obtained self-oscillations can be used to determine the process' parameters. The link between the space of process' parameters and the space of magnitudes and frequencies of self-oscillations is the Goldfarb principle given with (11), (see [13]).

$$G_P(j\omega) = -\frac{1}{G_N(X_m)} = -\frac{1}{P_N(X_m) + jQ_N(X_m)} \quad (11)$$

where $G_N(X_m) = P_N(X_m) + jQ_N(X_m)$ is the describing function of the nonlinear element, and $G_P(j\omega)$ is the process frequency characteristic. A relay with hysteresis is most commonly used for inducing self-oscillations and its describing function parameters are $P(X_m) = \frac{4C}{\pi X_m}\sqrt{1-\left(\frac{x_a}{X_m}\right)^2}$ and $Q(X_m) = -\frac{4C}{\pi X_m^2}x_a$, where C is relay output and x_a is hysteresis width. This element is used since it is insensitive to noise and can cause self-oscillations in any process whose Nyquist characteristic passes through the third quadrant. A matrix algorithm for determining unknown parameters of a general static transfer function can be found in [14]. The same reference includes modifications for astatic systems, systems with delays and discrete-time systems. When dealing with discrete-time systems, the value at which the relay switches might not be x_a but some value $x_a^* > x_a$. In this case, the self-oscillations should be analyzed a posteriori and x_a^* should be determined from the experiment and used in further calculations.

Identification by use of self-oscillations can also be used on a class of nonlinear systems as it will be demonstrated below, see also [5] and [6]. For equation

$$\alpha\ddot{x} = -\beta\dot{x}|\dot{x}| + \tau, \quad (12)$$

which describes yaw and surge dynamics, it is possible to derive expressions for unknown parameters based on magnitude, X_m, and frequency, ω, of self-oscillations. In 12 τ is surge force or yaw moment while α and β are parameters that have to be identified.

If the system is in oscillatory regime (due to the presence of the nonlinear element as in Fig. 5), and under the assumption that the oscillations are symmetric, output $x(t)$ and its derivations can be written as $x(t) = X_m\sin(\omega t)$, $\dot{x}(t) = X_m j\omega\sin(\omega t)$ and $\ddot{x}(t) = -X_m\omega^2\sin(\omega t)$. Unity feedback implies that $\tau = -G_N(X_m)x(t)$. By expanding the nonlinear term into a Fourier series and retaining only the first harmonic, the expressions for calculating α and β can be derived:

$$\alpha = \frac{P_N}{\omega^2} \quad (13)$$

$$\beta = -\frac{3\pi}{8}\frac{Q_N}{X_m\omega^2} \quad (14)$$

These equations can be used to determine unknown parameters in both yaw and surge dynamic models.

1) Identifying yaw model: For yaw model, equation (12) should be rewritten with $x = \psi$, $\tau = \tau_N$, $\alpha = I_r$ and $\beta = k_{r|r|}$. If the self-oscillation method is used on determining the unknown parameters, the input to the relay with hysteresis is

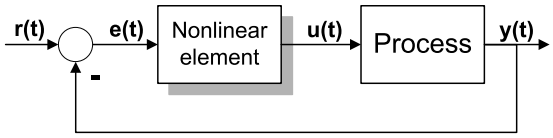

Fig. 5. Nonlinear element in a closed loop

$\psi_{REF}(t) - \psi(t)$ while the output is desired yaw moment τ_N. The inherent double integrator structure will ensure that the oscillations are symmetric around any ψ_{REF}.

2) Identifying surge model: For surge model, equation (12) should be rewritten with $x = u$, $\tau = \tau_X$, $\alpha = m_x$ and $\beta = k_{u|u|}$. For determining the surge model two approaches can be followed. If surge speed u can be measured, then the input to the nonlinear element is $\int_0^t (u_{ref}(t) - u(t))\, dt$. Introducing an extra integrator ensures symmetric self-oscillations around any u_{REF} (where usually $u_{REF} = 0$). Another approach, which is used in this paper, is using $d_{REF}(t) - d(t)$ as an input to the nonlinear element. Since $\dot{d} = -u\cos(\varphi) \approx -u$ if $\varphi \approx 0$, there is no need for introducing an extra integrator – only small angle with respect to surface has to be maintained. For both approaches the output of the nonlinear element is desired surge force τ_X.

The main disadvantage of the self-oscillation identification method is that the identified parameters are always uncertain. The reason for this is the fact that higher harmonics are neglected in the analysis leaving the derived expressions for the unknown parameters approximate. The main assumption in the self-oscillation analysis is that the process filters out higher harmonics effectively – this is the case for inertial systems, see [13]. A detailed analysis of errors that are introduced in I–SO method and methods on how to minimize them can be found in [5]. On the other hand, the I–SO method found it's application in tuning marine vehicles' controllers due to the fact that it is easily implementable, feasible in field conditions and time conservative.

IV. Controller Design

The control scheme is given in Fig. 4. Underwater vehicle is presented with a general dynamic and kinematic block while the sensors that are used are magnetic compass (giving ψ measurements) and laser based distance module (giving φ and d measurements). Kalman filter outputs are used in both angle and distance controllers.

The main objective in the paper is to develop a distance keeping controller. However, from (5) it is clear that the angle relative to the surface and the distance are coupled. This coupling can be resolved if the vehicle is kept at a constant angle, which is chosen to be 0. This is the reason why an angle φ controller should be developed also. Setting $\varphi_{REF} = 0$ ensures that $\varphi \approx 0$. That is why, prior to activating the distance d controller, angle φ controller is activated first.

Both angle and distance controllers which were implemented are of an I-PD form with a modification used for compensating the nonlinear term of the process (12). The controller (15) is appropriate because smooth output is produced even for abrupt changes of the referent signal. For the angle controller $x_{REF} = \varphi_{REF} = 0$, $x = \tilde{\varphi}$, $\dot{x} = \tilde{r}$ and $\tau = \tau_N$, while for the distance controller $x_{REF} = d_{REF}$, $x = \tilde{d}$, $\dot{x} = -\tilde{u}\cos\tilde{\varphi}$ and $\tau = \tau_X$. Tilde symbol denotes the Kalman filter estimates.

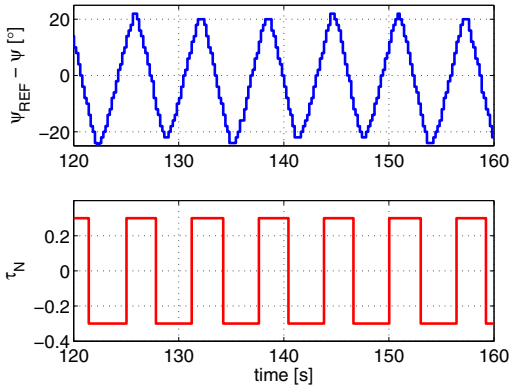

Fig. 6. The self-oscillation experiment for yaw degree of freedom

$$\tau(t) = K_I \int_0^t [x_{REF}(t) - x(t)]\, dt - K_P x(t) - K_D \dot{x}(t) \tag{15}$$

Parameters of both controllers are set so that the closed loop transfer function for corresponding feedback loop is equal to the model function $G_m(s) = \frac{1}{a_3 s^3 + a_2 s^2 + a_1 s + 1}$ which is stable. In that case, the controller parameters are given with $K_I = \frac{\alpha}{a_3}$, $K_P = \frac{a_1}{a_3}\alpha$ and $K_D = \frac{a_2}{a_3}\alpha - \beta\,|\dot{x}(t)|$, where α and β are determined from the self-oscillation experiments. It is clear that the controller parameters are time varying. A detailed stability analysis of the closed loop is given in [6] and the main result is that the structural and robust stability can be ensured by limiting the derivation channel action.

V. Experimental Results

A. Yaw DOF Self-Oscillations

The self-oscillation experiment for yaw degree of freedom is shown in Fig. 6. Relay switching was set to $x_a = 10°$, but the a posteriori analysis showed it was in fact $x_a^* = 12.62°$ (because of the discrete-time nature). The relay output is more or less symmetric which indicates that the disturbance during the experiment was negligible. The self-oscillation parameters from the experiment are $X_m = 22.1°$ and $\omega = 0.997\text{s}^{-1}$.

B. Surge DOF Self-Oscillations

After the angle controller is set using the parameters from the yaw degree self-oscillation experiment, surge degree of freedom can be identified. The experimental results are shown in Fig. 7 with relay switching set to $x_a = 10\text{cm}$, but the a posteriori analysis showed it was in fact $x_a^* = 12.33\text{cm}$. In this case, relay output is somewhat asymmetric which is a result of influence of the tether that presents significant

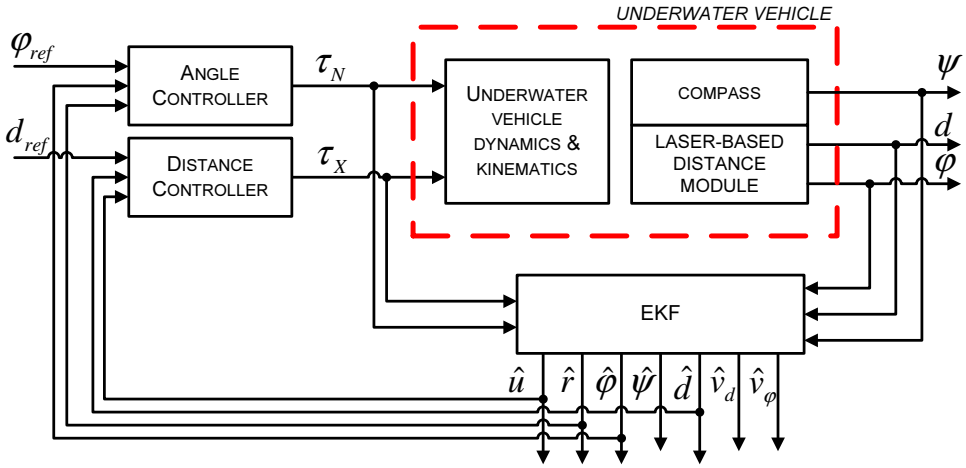

Fig. 4. Control scheme

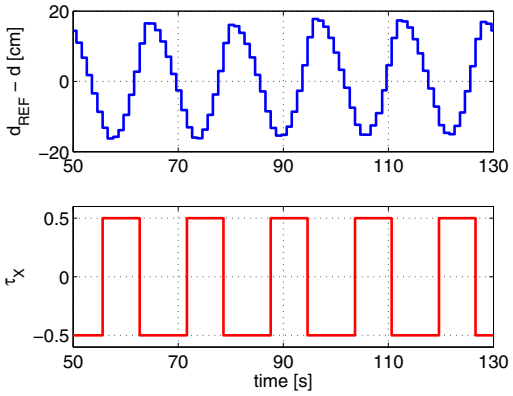

Fig. 7. The self-oscillation experiment for surge degree of freedom

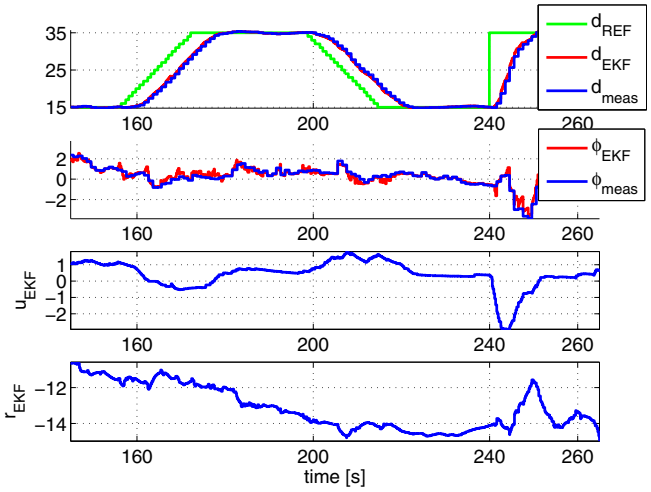

Fig. 8. Responses of the closed loop system to the ramp and step referent distance change and constant angle $\varphi_{REF} = 0$

disturbance. It can also be shown that this asymmetry does not affect significantly the precision of determining the surge model parameters. The self-oscillation parameters from the experiment are $X_m = 16.22\text{cm}$ and $\omega = 0.393\text{s}^{-1}$.

C. Distance Keeping

Fig. 8 demonstrates the responses of the closed loop system to the ramp and step referent distance change and constant angle $\varphi_{REF} = 0$ with the I-PD control algorithm. It can be seen that the Kalman filter estimates the distance value well in between the measurements. Also, surge (u_{EKF}) and yaw (r_{EKF}) speed estimates are smooth and show that the disturbance was significant during the experiments (mostly due to the influence of the tether). However, the controller preforms well in transient as well as the steady state. The case where measurements are not available for quite some time are shown in Fig. 9. At times $t = 435\text{s}$ and $t = 455\text{s}$ the laser dots from the laser-based distance module become unavailable due to a disturbance and they appear back at $t = 440\text{s}$ and $t = 460\text{s}$, respectively. During this time, the Kalman filter estimated the behavior of the vehicle properly and control was not lost.

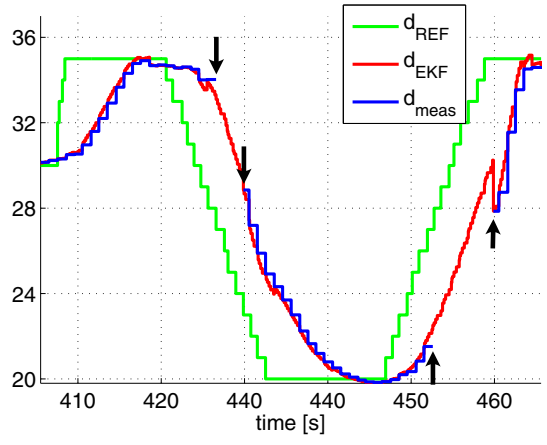

Fig. 9. Responses of the closed loop system to distance change in case of missing measurements

VI. Conclusion

The work presented in this paper describes the use of self-oscillation experiments for tuning Kalman filter parameters. The process that is observed is a distance keeping for underwater vehicles based on a laser system which projects two dots on a surface. The measurements obtained from this system were used to determine the distance and the angle with respect to the surface. Since the refresh frequency of the laser system is lower than that of the control system, Kalman filtering is needed. A discrete extended Kalman filter has been designed in order to improve control. A novel approach for determining unknown parameters of nonlinear systems was applied to determine dynamic equations of the Kalman filter. The implemented controller was nonlinear of I-PD type which ensured the smooth controller output. The results show that the proposed procedure is feasible in practice and gives satisfactory results.

Acknowledgment

The work was carried out in the framework of the research project "RoboMarSec - Underwater robotics in sub-sea protection and maritime security" supported by the Ministry of Science, Education and Sport of the Republic of Croatia (Project No.036-0362975-2999). The authors would like to thank Dula Nad, dipl. ing. and Nenad Trifunovic for acting as a disturbance during the testing of the Kalman filter performance.

References

[1] M. Caccia, "Laser-triangulation optical-correlation sensor for ROV slow motion estimation," *IEEE Journal of Oceanic Engineering*, vol. 31(3), pp. 711–727, 2006.

[2] G. Karras, D. Panagou, and K. Kyriakopoulos, "Target-referenced localization of an underwater vehicle using a laser-based vision system," *Proc. of the OCEANS 2006 Conference*, 2006.

[3] G. Karras and K. Kyriakopoulos, "Localization of an underwater vehicle using an IMU and a laser-based vision system," *Proc. of the 15th Mediterranean Conference on Control and Applications*, 2007.

[4] F. Lewis and V. Syrmos, *Optimal control*. New York, NY, USA: John Wiley & Sons, Inc., 1995.

[5] N. Miskovic, Z. Vukic, M. Barisic, and P. Soucacos, "AUV identification by use of self-oscillations," *Proc. of the CAMS'07 Conference*, 2007.

[6] N. Miskovic, Z. Vukic, and E. Omerdic, "Control of UUVs based upon mathematical models obtained from self-oscillations experiments," *Proc. of the NGCUV'08 Conference*, 2008.

[7] M. Bibuli, G. Bruzzone, M. Caccia, N. Miskovic, and Z. Vukic, "Self-oscillation based identification and heading control of unmanned surface vehicles," *Proc. of the RAAD'08 Conference*, 2008.

[8] T. Fossen, *Guidance and Control of Ocean Vehicles*. Chichester: John Wiley & Sons, 1994.

[9] M. Caccia, G. Indiveri, and G. Veruggio, "Modelling and identification of open-frame variable configuration underwater vehicles," *IEEE Journal of Ocean Engineering*, vol. 25(2), pp. 227–240, 2000.

[10] G. Welch and G. Bishop, *An Introduction to the Kalman filter*. Chapell Hill: University of North Carolina, 2006.

[11] K. J. Åstrom and Hagglund, "Automatic tuning of simple regulators with specifications on phase and amplitude margins," *Automatica*, vol. 20, p. 645, 1984.

[12] N. Miskovic, Z. Vukic, and M. Barisic, "Identification of underwater vehicles for the purpose of autopilot tuning," *Underwater Vehicles*, pp. 327–346, 2009.

[13] Z. Vukic, L. Kuljaca, D. Donlagic, and S. Tesnjak, *Nonlinear Control Systems*. New York: Marcel Dekker, 2003.

[14] N. Miskovic, Z. Vukic, M. Barisic, and B. Tovornik, "Autotuning autopilots for micro-ROVs," *Proc. of the 14th Mediterranean Conference on Control and Applications*, 2006.